New opportunities for ultrafast and highly enantio-sensitive imaging of chiral nuclear dynamics enabled by synthetic chiral light – Supplementary Information

David Ayuso

Department of Physics, Imperial College London, SW7 2AZ London, United Kingdom.
Max-Born-Institut, Max-Born-Str. 2A, 12489 Berlin, Germany.
d.ayuso@imperial.ac.uk

Here we describe the method applied to model the ultrafast electronic response of the chiral molecule H_2O_2 to synthetic chiral light[1]. The electric-field vector of the laser field has three orthogonally polarized components: it is elliptically polarized in the xy plane with frequency ω, and it has a 2ω frequency component that is linearly polarized along z (see Fig. 1 of the main text):

$$\mathbf{E}(t) = a_0(t)\left[E_x \cos(\omega t)\hat{\mathbf{x}} + E_y \sin(\omega t)\hat{\mathbf{y}} + E_z \cos(2\omega t + \phi_{2\omega})\hat{\mathbf{z}}\right], \tag{S1}$$

where a_0 is the temporal envelope, and E_x, E_y and E_z are the field amplitudes, with $E_x >> E_y$ and $E_x >> E_z$. The spatial dependence of E_x, E_y and E_z is given in the main text, but we shall omit it here for simplicity. Because the E_y and E_z are weak, they can be treated perturbately, and thus the polarization driven by this field in a medium of randomly oriented chiral molecules can be written as

$$\mathbf{P}(t) = P_x^a(t)\hat{\mathbf{x}} + [P_y^a(t) + P_y^c(t)]\hat{\mathbf{y}} + [P_z^a(t) + P_z^c(t)]\hat{\mathbf{z}}, \tag{S2}$$

where P_x^a, P_y^a, P_y^c, P_z^a and P_z^c are the achiral and chiral contributions to the light-induced polarization. The achiral contributions are identical in left- and right-handed molecules, whereas the chiral contributions are exclusive of chiral media and have the same intensity but opposite phase in opposite molecular enantiomers. Note that P_x^a is parallel to the strong-field component E_x, and thus it is solely driven by this field component, i.e. P_x^a is not affected by the weak components E_y and E_z. Likewise, the chiral contribution P_z^c relies on the interplay of the molecules with E_x and E_y and it is not affected by E_z, and the achiral contribution P_z^a involves E_x and E_z, but not E_y. The corresponding achiral and chiral multi-photon pathways[1] are depicted in Fig. 2 of the main text. Note also that P_y^a and P_y^c are parallel to the propagation direction y, and therefore they cannot generate a macroscopic harmonic signal in the far field. Thus, the enantio-sensitive macroscopic response of the chiral medium relies on the interference between P_z^a and P_z^c.

Synthetic chiral light enables full control over the interference between P_z^a and P_z^c, allowing us to enhance the enantio-sensitive response in one molecular enantiomer while fully quenching it in its mirror twin. Indeed, P_z^a and P_z^c depend linearly on E_z and E_y, respectively, i.e. $P_z^a \propto E_z$ and $P_z^c \propto E_y$. Furthermore, the phase of P_z^a can be controlled with the two-colour phase delay

$\phi_{2\omega}$. Thus, by controlling the relative amplitude and two-colour phase delay, we get full control over the interference.

We have modelled the interaction of different nuclear configurations of H_2O_2 with synthetic chiral light using the state-of-the-art implementation of real-time time-dependent density functional theory in Octopus[2–5]. The light-induced polarization in the randomly oriented ensemble (Eq. S2) was obtained by averaging over 200 molecular orientations as described in the main text. We used the local-density approximation[6–8] to account for electronic exchange and correlation effects, and the averaged-density self-interaction correction[9] to ensure an accurate description of the long-range part of the electronic density. The 1s orbitals of the oxygen atoms were described via pseudo-potentials. We used a uniform real-space grid in a spherical basis set of radius 30.7 a.u., with spacing between neighbouring points of 0.4 a.u., and a complex absorbing potential with width 20 a.u. and height -0.2 a.u.

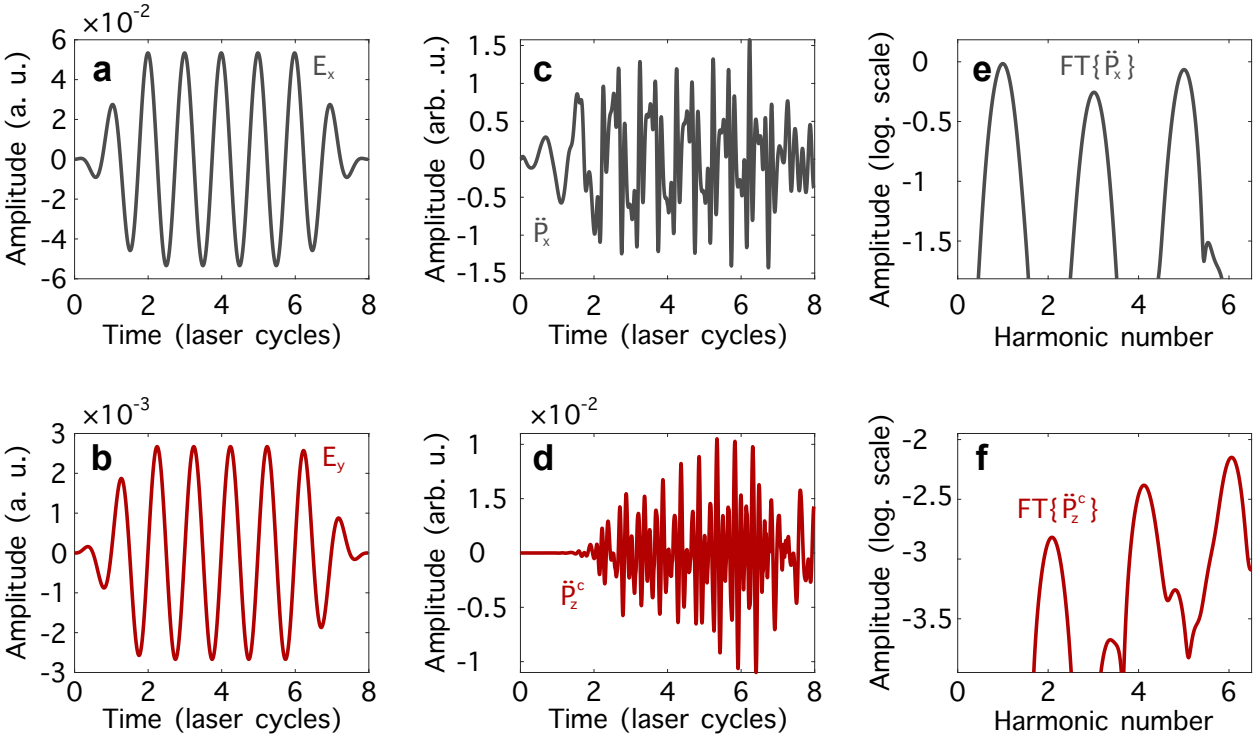

Figure S1: **Electronic response of H_2O_2 to an elliptically polarized field. a,b,** Electric-field amplitude of the x-polarized (**a**) and y-polarized (**b**) components of the elliptically polarized driving field. We used a fundamental wavelength of 400nm, intensity 10^{14}W·cm^{-2}, and a sine-squared flat-top envelope of 8 laser cycles (10.7 fs): 2 cycles to rise up, 4 cycles of constant intensity, and 2 cycles to go down. **c,d,** Second derivative of the (achiral) x-polarized (**c**) and chiral z-polarized (**d**) components of the induced polarization driven in the left-handed equilibrium geometry of randomly oriented H_2O_2. **e,f,** Fourier transform of the second derivative of the (achiral) x-polarized (**e**) and chiral z-polarized (**f**) components of the induced polarization. To reduce the numerical noise in the harmonic spectrum, we applied a Gaussian filter in the time domain before doing the Fourier transform. This filter had a full width at half maximum of 2.7 fs and was centered at the center of the envelope.

As above described, P_z^c relies on the interplay of the molecules with the E_x and E_y field components, and it is not affected by E_z. Thus, we have calculated the ultrafast electronic response of H_2O_2 to an elliptically polarized driving field with wavelength of 400nm, intensity 10^{14}W·cm^{-2}, and 8 cycles of duration. The x and y components of the driving field are shown in Figs. S1a,b. Figs. S1c,d show the relevant components of the acceleration of the induced polarization, i.e. the second derivative of the polarization components P_x (Fig. S1c) and P_z^c (Fig. S1d) driven by the field in the left-handed (randomly oriented) equilibrium geometry of H_2O_2 (see Fig. 3 of the main text). As above described, P_z^c is exclusive of chiral media, and its phase records the handedness of the medium. The values shown in Fig. S1c are strong because P_z^c is driven by purely electric-dipole interactions, and well above the numerical noise of the simulations, which is 10 orders of magnitude weaker than the obtained signal (to estimate the numerical noise in the simulations, we have run additional calculations for the planar configuration of H_2O_2 with dihedral angle $180°$). Figs. S1e,f show the induced polarization in the frequency domain, i.e. the Fourier transform of the time-dependent response shown in Figs. S1c,d. Note that the (achiral) x-polarized component of the induced polarization contains odd harmonic frequencies, whereas the chiral component of the z-polarized response contains even harmonic frequencies[1].

To compute the achiral polarization component P_z^a driven in the (randomly oriented) equilibrium geometry of H_2O_2, we have run simulations including the x and z polarization components of the driving field, see Figs. S2a,b, and neglecting E_y. We have considered 4 values of the two-colour phase delay, see Fig. S2b. The second derivative of P_x and P_z^a is presented in Figs. S2c,d. Note that P_x is indeed solely driven by the strong-field component of the driving field, and thus we get the same results in the simulations with the elliptical (Fig. S1c) and two-colour (Fig. S2c) driving fields. Note also that, as expected, the two-colour phase delay $\phi_{2\omega}$ controls the phase of P_z^a. The Fourier components of the induced polarization are shown in Figs. S2e,f.

We can model the ultrafast electronic response of the medium to a (3D) locally chiral field with arbitrary (but weak) amplitudes E_y and E_z and phase delay $\phi_{2\omega}$ using the perturbative treatment above described, and the values presented in Figs. S1 and S2. This perturbative treatment allows us to find the optimum laser parameters which maximize the enantio-sensitive response of the molecules analytically, without having to run numerical simulations using 3D fields with varying amplitudes and phase delay, thus reducing dramatically the computational cost.

We have run simulations for dihedral angles $79°$, $112°$ and $146°$ (the induced polarization for dihedral angles $214°$, $248°$ and $281°$ was obtained using symmetry considerations). For each nuclear geometry, we ran one set of simulations using the elliptically polarized driving field presented in Figs. S1a,b to compute P_z^c, and 4 sets of simulations using the two-colour fields presented in

Figs. S2a,b, with $\phi_{2\omega} = 0$, 0.25π, 0.5π and 0.75π (the induced polarization for $\phi_{2\omega} = \pi$, 1.25π, 1.5π and 1.75π was obtained using symmetry considerations). For each molecular geometry and laser configuration, we ran 200 simulations using different molecular orientations in order evaluate the response of the randomly oriented ensemble, as described in the main text. That is, each molecular geometry required running 1000 simulations, so we ran 3000 simulations in order to produce the results presented in the main text. Each individual simulation took, approximately, 1 day in a single processor.

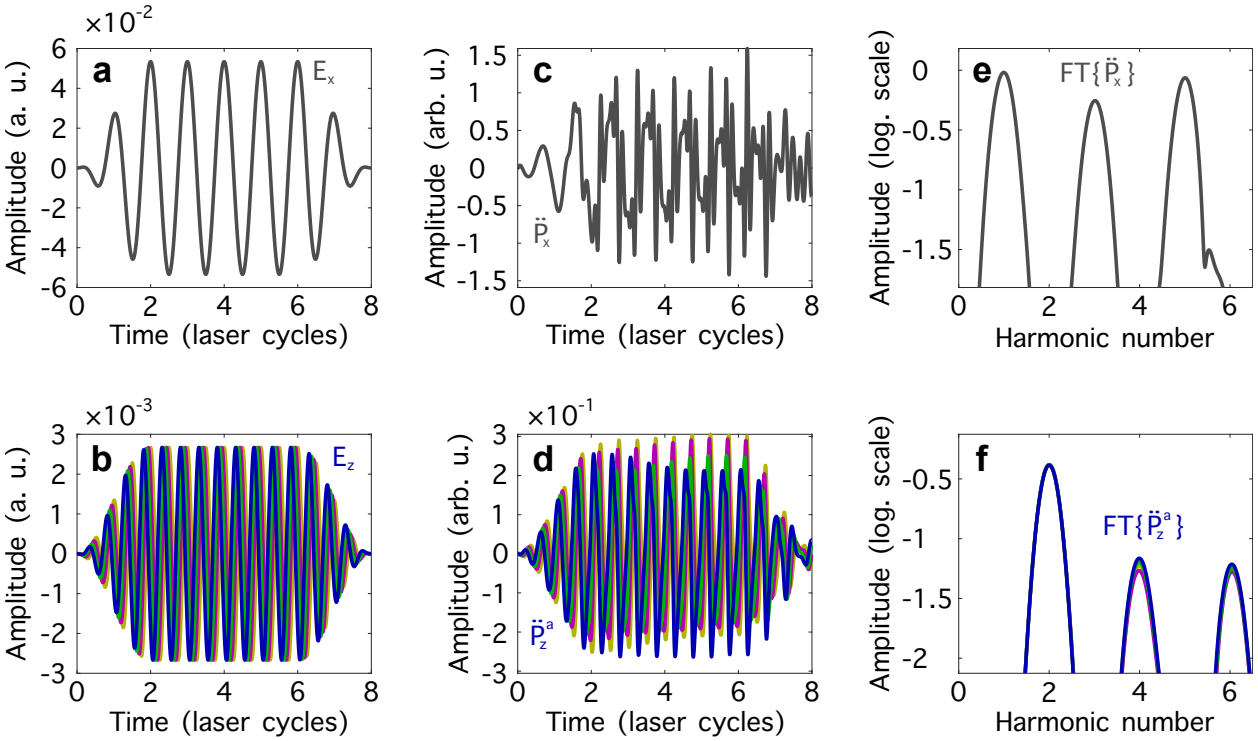

Figure S2: **Electronic response of H_2O_2 to a cross-polarized two-colour field. a,b,** Electric-field amplitude of the x-polarized (**a**) and z-polarized (**b**) components of the two-colour driving field. We used a fundamental wavelength of 400nm, intensity 10^{14}W·cm^{-2}, two-colour delay $\phi_{2\omega} = 0$, 0.25π, 0.5π and 0.75π, and a sine-squared flat-top envelope of 8 laser cycles (10.7 fs): 2 cycles to rise up, 4 cycles of constant intensity, and 2 cycles to go down. **c,d,** Second derivative of the (achiral) x-polarized (**c**) and achiral z-polarized (**d**) components of the induced polarization driven in the left-handed equilibrium geometry of randomly oriented H_2O_2. **e,f,** Fourier transform of the second derivative of the (achiral) x-polarized (**e**) and achiral z-polarized (**f**) components of the induced polarization. To reduce the numerical noise in the harmonic spectrum, we applied a Gaussian filter in the time domain before doing the Fourier transform. This filter had a full width at half maximum of 2.7 fs and was centered at the center of the envelope.

References

1. Ayuso, D. *et al.* Synthetic chiral light for efficient control of chiral light–matter interaction. *Nature Photonics* **13**, 866–871 (2019).

2. Marques, M. A., Castro, A., Bertsch, G. F. & Rubio, A. Octopus: a first-principles tool for excited electron–ion dynamics. *Computer Physics Communications* **151**, 60 – 78 (2003).

3. Castro, A. *et al.* octopus: a tool for the application of time-dependent density functional theory. *Physica Status Solidi (b)* **243**, 2465–2488 (2006).

4. Andrade, X. *et al.* Real-space grids and the octopus code as tools for the development of new simulation approaches for electronic systems. *Phys. Chem. Chem. Phys.* **17**, 31371–31396 (2015).

5. Tancogne-Dejean, N. *et al.* Octopus, a computational framework for exploring light-driven phenomena and quantum dynamics in extended and finite systems. *The Journal of Chemical Physics* **152**, 124119 (2020).

6. Dirac, P. A. M. Note on exchange phenomena in the thomas atom. *Mathematical Proceedings of the Cambridge Philosophical Society* **26**, 376–385 (1930).

7. Bloch, F. Bemerkung zur elektronentheorie des ferromagnetismus und der elektrischen leitfähigkeit. *Zeitschrift für Physik* **57**, 545–555 (1929).

8. Perdew, J. P. & Zunger, A. Self-interaction correction to density-functional approximations for many-electron systems. *Phys. Rev. B* **23**, 5048–5079 (1981).

9. Legrand, C., Suraud, E. & Reinhard, P.-G. Comparison of self-interaction-corrections for metal clusters. *Journal of Physics B: Atomic, Molecular and Optical Physics* **35**, 1115–1128 (2002).